

Multispectral filter array and demosaicking for pathological images

Kazuma Shinoda*, Shu Ogawa*, Yudai Yanagi*, Madoka Hasegawa*, Shigeo Kato*,
Masahiro Ishikawa†, Hideki Komagata†, and Naoki Kobayashi†

* Graduate School of Engineering, Utsunomiya University, Utsunomiya, Japan

E-mail: shinoda@is.utsunomiya-u.ac.jp Tel: +81-28-689-6267

† Faculty of Health and Medical Care, Saitama Medical University, Hidaka, Japan

Abstract—A single-shot multispectral camera equipped with a filter array has the potential to promote a fast and low-cost multispectral imaging system. We focus on the design of a multispectral filter array and demosaicking in this paper and propose a pathology-specific multispectral imaging system. The spectral sensitivities and patterns of the filter array are optimized by using training data of real pathological tissues. The mosaicked image is demosaicked by considering the designed filter array. We show the effectiveness of the proposed imaging system by comparing the recovered spectrum and RGB image with conventional methods.

I. INTRODUCTION

Multispectral images (MSIs) have been studied in the fields of remote sensing, medical applications, and digital archiving. As an example of a medical application, a color correction method for hematoxylin and eosin (H&E)-stained pathological images using a 16-band multispectral microscope camera system has been reported [1], [2]. The pathological diagnosis deals with the examination of tissues and cells under a microscope. Fig. 1 shows an example of a pathological image, a 20× optically zoomed liver stained with H&E, where the dark dots indicate the nuclei. Color reproduction and morphological characteristics of the nuclei/cells are important for the pathological diagnosis, and a study [3] has examined the color differences in the nuclei in a multispectral imaging system. Since the spectral features of pathological tissues can be estimated from MSI, some studies have explored the digital staining of pathological tissues [4], [5]. However, limitations persist in the techniques for capturing MSI because of the complexity of assembling prisms or multiple sensor arrays in order to detect signals. Inspired by the application of color filter arrays (CFAs) to commercial digital RGB cameras, multispectral filter arrays (MSFAs) have been studied to solve this problem.

Two examples of MSFAs are shown in Fig. 2. Brauers et al. [6] proposed a six-band MSFA arranged in 3×2 pixels in a straightforward manner intended for faster linear interpolation. Monno et al. [7] proposed a five-band MSFA and determined that the sampling density of the G-band data was higher than that of the other spectral bands because the human eye is more sensitive to the G-band than to the other spectral bands. In recent years, other approaches have been studied in [8]. Since these studies design MSFA for reducing the spectral estimation error or the color difference of CIE ΔE , MSFA will also be

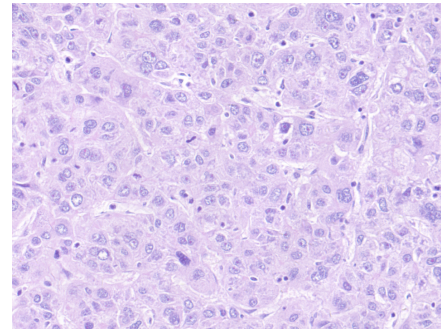


Fig. 1: Example of a pathological image. H&E-stained liver, 20× magnification, 1920 × 1440, RGB image.

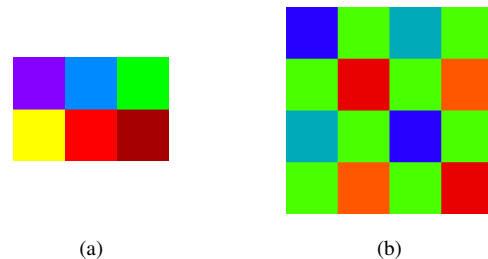


Fig. 2: Examples of MSFAs. (a) Brauers et al. [6] (b) Monno et al. [7].

effective for pathological images. However, the MSFA design and the demosaicking method suited for a specific application such as pathological images have not been studied. As we can see from Fig. 1, the color distribution is biased toward blue and magenta because the pathological image consists of a limited number of human cells and its spectral distribution is also very limited. Therefore, for pathological application of MSFA techniques, the number of color filters of MSFA can be reduced depending on the spectral distribution of the pathological image, and thus, the demosaicked image quality can be improved.

Here, we propose a new MSFA design method [9] and demosaicking [10], but we have not examined their effect in detail with respect to a specific application. In this study, we apply these methods to H&E-stained pathological images and

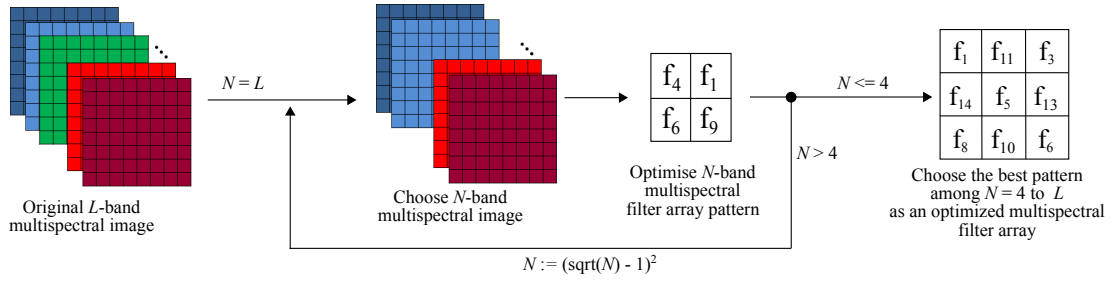


Fig. 3: Design flow for a multispectral filter array.

clarify the optimized MSFA pattern and demosaicked quality. We use a 51-band MSI, which is captured by a multishot multispectral camera, as the original image. First, measured wavelengths and filter array patterns are designed to reduce the recovered image quality by using our prior work [9]. After optimizing the MSFA, we apply multispectral local directional interpolation (MLDI) [10] for demosaicking. We finally show that the proposed MSFA pattern outperforms the conventional methods.

The rest of this paper is organized as follows: In Section II, we describe our design method for MSFA. In Section III, we explain our demosaicking method. We discuss the experiment used for testing the proposed method and the results in Section IV. Section V presents our conclusions.

II. FILTER ARRAY OPTIMIZATION BASED ON PATHOLOGICAL IMAGES

First, we explore a method for optimizing the MSFA design based on pathological images. The proposed method uses a 51-band pathological MSI as the original image and simulates mosaicking and demosaicking on a computer. The proposed design flow of MSFA is shown in Fig. 3 [9]. We explore the MSFA pattern iteratively to minimize the demosaicked mean square error (MSE). The proposed flow consists of two parts: wavelength optimization and spatial pattern optimization. In the wavelength optimization procedure, N bands are chosen from L bands of the MSI so that the MSE is minimized. Here, L denotes the number of original bands, $N \leq L$, and spatial mosaicking is not applied to the N -band MSI. After choosing N bands, we optimize the spatial pattern of MSFA by using simulated annealing [11]. After the optimized N -band MSFA is obtained, N is decreased, and then, these procedures are repeated. In this study, $N = x^2$ and x denotes an arbitrary positive integer. The detailed procedures for wavelength optimization and pattern optimization are described in Section II-A and Section II-B, respectively.

In the proposed design flow, some spectral bands of the original MSI are not measured by MSFA because $N \leq L$. If the number of bands of MSFA is increased, the spatial sampling interval of each band becomes sparser, which in turn leads to a degradation of the demosaicking quality. Since the number of bands of the optimized MSFA is not always L , we assume $N \leq L$ and calculate MSEs for $N = 4$ to L .

The L -band MSI has to be recovered from the N -band mosaicked MSI, but conventional demosaicking methods [6], [7], [10] cannot interpolate such unmeasured bands. Therefore, in the proposed MSFA design flow, we apply Brauers' demosaicking [6] for recovering the N -band MSI and then, apply Wiener estimation [12] for recovering the L -band MSI from the N -band MSI. Here, the Wiener estimation matrix consists of the first-order Markov process with the correlation coefficient $\rho = 0.9995$ [13], [14].

A. Wavelength optimization for MSFA

In the wavelength optimization procedure, we choose N wavelengths from L . When choosing N from L , the total number of combinations is ${}_LC_N$; therefore, it is impractical to explore all the combinations when $L \gg N$. Hence, we choose the N -band MSI from the L -band MSI iteratively as follows: $I^{(n)}$ denotes an n -band MSI; $I_i^{(n-1)} (i = 1, \dots, n)$ represents an $n-1$ -band MSI, which removes i -th band from $I^{(n)}$; and $f(I^{(n)})$ indicates an MSE between the estimated L -band MSI from $I^{(n)}$ and the original MSI. n is initialized to L , and we iteratively calculate $I^{(n-1)}$ as follows:

$$I^{(n-1)} = \arg \min_{I_i^{(n)}} f(I_i^{(n)}) \quad (i = 1, \dots, n). \quad (1)$$

After $n := n-1$, this process is repeated until $n = N$. Finally, the optimized N -band MSI can be obtained.

B. Pattern optimization for MSFA

The spatial filter pattern is optimized from the obtained N -band MSI in Section II-A. The pattern optimization procedure determines the spatial arrangement of each of the N filters. Here, let the MSFA size be $x \times x$. For example, if an arbitrary $x \times x$ MSFA is given, the mosaicked image can be calculated from the N -band MSI, and then, the demosaicked L -band MSI can be calculated by using Brauers' demosaicking and Wiener estimation. Thus, the MSE between the demosaicked and the original MSI can be obtained if a pattern of $x \times x$ MSFA is given. The global minimum of MSE can be obtained if all MSFA patterns are examined, but such a calculation is impractical. To optimize the MSFA pattern based on MSE, we use simulated annealing. The optimization details are as follows:

The set of center wavelengths (f_1, f_2, \dots, f_N) is given as a precondition from the wavelength optimization procedure. For

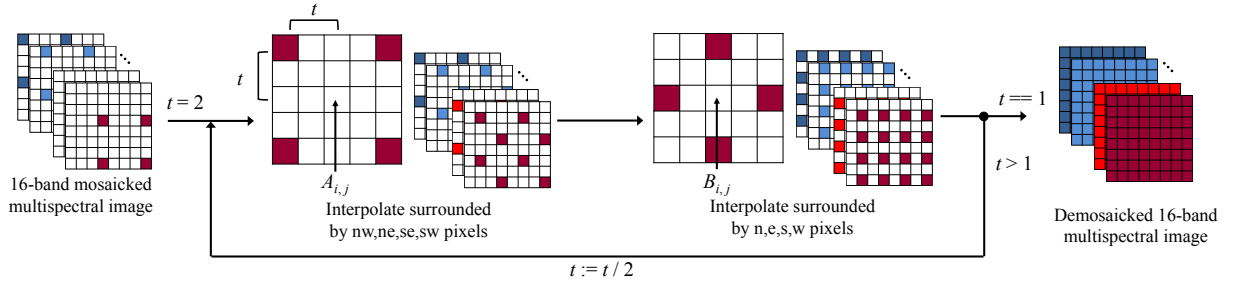


Fig. 4: Main flow of MLDI (Step 1).

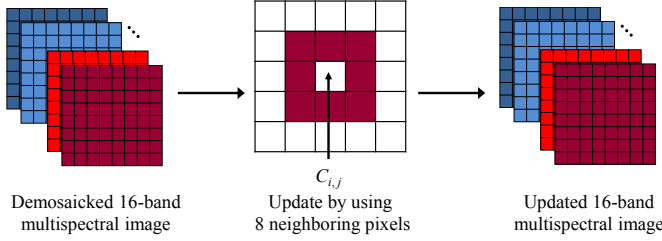


Fig. 5: Updating the interpolated pixels after MLDI (Step 2).

initialization, the filters are randomly arranged in an MSFA block. Let S be the current state of the MSFA, and let the neighboring state S' be created by swapping two arbitrary filters. The acceptance criterion for the neighboring states is determined by comparing the MSE as follows:

$$p(\Delta, T) = \begin{cases} 1 & (\Delta \geq 0) \\ \exp^{-\frac{\Delta}{T}} & (\Delta < 0) \end{cases} \quad (2)$$

$$\Delta = \text{MSE}_S - \text{MSE}_{S'}, \quad (3)$$

where T denotes the temperature, MSE_S represents the MSE of pattern S , and $\text{MSE}_{S'}$ indicates the MSE of pattern S' . The annealing schedule is repeated for $T := 0.999 \cdot T$, where T is set to 1 in the initialization and is terminated at 10,000 iterations. Finally, we adopt pattern S with the smallest value of MSE_S as the optimized MSFA.

III. DEMOSAICKING FOR MULTISPECTRAL FILTER ARRAY

In this section, we explain the demosaicking algorithm of MLDI [10]. Fig. 4 shows an overview of MLDI. First, the center pixel surrounded by the north-west (nw), north-east (ne), south-east (se), and south-west (sw) pixels is interpolated by considering the gradient among the four abovementioned neighboring pixels. Then, the center pixel surrounded by the north (n), east (e), south (s), and west (w) pixels is interpolated. This process is repeated until all the pixels are interpolated.

Then, the interpolated pixels are modified as shown in Fig. 5. Fig. 4 uses four neighboring pixels to calculate the gradient, but we can use eight neighboring pixels after Step 1 of MLDI. Therefore, we modify the already-interpolated pixels by using eight neighboring pixels in Step 2.

A. MLDI Step 1

Let the interpolation target band be A , the reference band be R , and the position of the interpolation target pixel be (i, j) . Here, “reference” means a band where the measured pixel at (i, j) exists. First, the inter-band difference between the target and the reference bands is calculated as follows:

$$d^{nw} = A_{i-t, j-t} - (R_{i, j} + R_{i-2t, j-2t})/2, \quad (4)$$

where t denotes the square root of the block distance between the target pixel and the measured (or already-interpolated) pixel, and nw represents the north-west direction from the target pixel. As in (4), the north-east, south-east, and south-west inter-band differences are calculated as d^{ne} , d^{se} , and d^{sw} , respectively.

The gradient weight is calculated as follows:

$$w^{nw} = 1/(|A_{i-t, j-t} - A_{i+t, j+t}| + |R_{i-2t, j-2t} - R_{i, j}| + |\tilde{R}_{i-t, j-t} - R_{i, j}| + \varepsilon), \quad (5)$$

where \tilde{R} denotes a temporarily interpolated pixel by Bilinear interpolation and ε represents a small value to avoid zero division. The inter-band difference considering the gradient can be calculated from d and w as follows:

$$\bar{d} = \frac{w^{nw} d^{nw} + w^{ne} d^{ne} + w^{se} d^{se} + w^{sw} d^{sw}}{w^{nw} + w^{ne} + w^{se} + w^{sw}}. \quad (6)$$

Finally, the target pixel is obtained as follows:

$$\bar{A}_{i, j} = R_{i, j} + \bar{d}. \quad (7)$$

Next, let the interpolation target be B , as shown in Fig. 4. $B_{i, j}$ is interpolated using four neighboring pixels located in the north, south, west, and east directions. The inter-band difference between the target and the reference bands in the north is calculated as follows:

$$d^n = B_{i, j-t} - (R_{i, j} + R_{i, j-2t})/2, \quad (8)$$

Then, the gradient weight is calculated as follows:

$$\begin{aligned}
 w^n &= 1/(|R_{i,j-2t} - R_{i,j}| \\
 &+ \sum_{k=1}^t |M_{i,j-(t+(k-1))} - M_{i,j+(t-(k-1))}| \\
 &+ \sum_{k=1}^t W_k |M_{i-k,j-2t} - M_{i-k,j}| \\
 &+ \sum_{k=1}^t W_k |M_{i+k,j-2t} - M_{i+k,j}| + \varepsilon) \quad (9)
 \end{aligned}$$

$$W_k = \frac{\exp(-k^2/(2\sigma^2))}{2 \sum_{l=1}^t \exp(-l^2/(2\sigma^2))}, \quad (10)$$

where M denotes a pixel in the mosaicked image, σ represents the constant parameter, and W_k indicates the weight factor whose summation is 0.5. We set σ to 0.5 in this study. The east, south, and west gradient weights are calculated as w^e , w^s , and w^w , respectively. The inter-band difference considering the gradient can be calculated from d and w as follows:

$$\bar{d} = \frac{w^n d^n + w^e d^e + w^s d^s + w^w d^w}{w^n + w^e + w^s + w^w}. \quad (11)$$

Finally, the target pixel is obtained as follows:

$$\bar{B}_{i,j} = R_{i,j} + \bar{d}. \quad (12)$$

After interpolating A and B , we repeat the process by using $t = t/2$ until $t = 1$.

B. MLDI Step 2

The first step of MLDI uses the four neighboring pixels in the same band. For improving the interpolation accuracy, we modify all the interpolated pixels C by using eight neighboring pixels, as shown in Fig. 5. First, the inter-band difference between the target and the reference bands is calculated as follows:

$$d^{nw} = C_{i-1,j-1} - R_{i-1,j-1}, \quad (13)$$

The other differences in the ne, se, sw, n, e, s, and w directions are also calculated. The gradient weight can be calculated in the same manner as (5) and (9). The inter-band difference considering the gradient can be calculated from d and w as follows:

$$\begin{aligned}
 \bar{d} &= (w^{nw} d^{nw} + w^{ne} d^{ne} + w^{se} d^{se} + w^{sw} d^{sw} \\
 &+ w^n d^n + w^e d^e + w^s d^s + w^w d^w) \\
 &/ (w^{nw} + w^{ne} + w^{se} + w^{sw} \\
 &+ w^n + w^e + w^s + w^w). \quad (14)
 \end{aligned}$$

Finally, the target pixel is obtained as follows:

$$\bar{C}_{i,j} = R_{i,j} + \bar{d}. \quad (15)$$

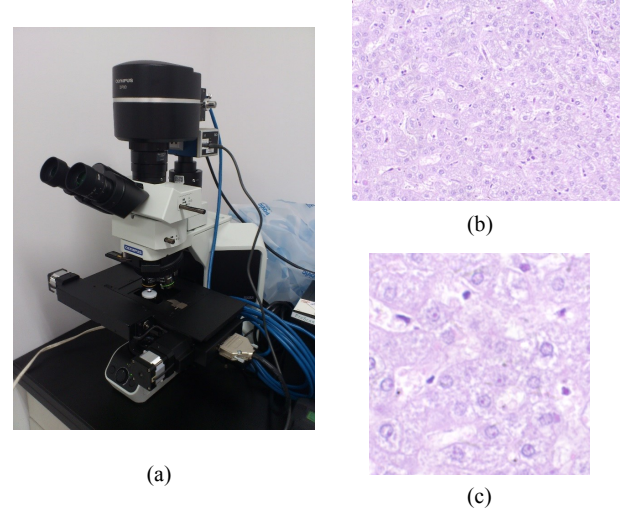


Fig. 6: Multishot multispectral imaging system and test image. (a) Microscope equipped with multishot multispectral imaging system (b) H&E-stained liver, 20 \times magnification, RGB image, 1920 \times 1440 pixels. (c) 512 \times 512 pixels cropped from the center of 1920 \times 1440 pixels. This image is used for MSFA design and demosaicking test.

TABLE I: PSNR (dB) of demosaicked MSI.

MSFA size	2 \times 2	3 \times 3	4 \times 4
Proposed	28.287	31.432	31.259
Shinoda et al. [15]	24.317	30.950	30.973
Bayer	24.309	31.009	30.970
Raster	24.317	30.952	30.820

IV. EXPERIMENTAL RESULTS

We show the validation of the proposed method by using pathological MSI. For the experiment, we captured a 51-band MSI with a microscope and a multishot multispectral imaging system. Fig. 6 (a) shows the optical microscope (Olympus, BX53) equipped with a multispectral imaging system. The imaging system uses liquid crystal tunable filters (CRi, Varispec VIS), and monochrome CCD (Point Grey, Grasshopper 3). The pathological tissue is of an H&E-stained liver (US Biomax, Hepatocellular Carcinoma Tissue Array C054) and is shown in Fig. 6 (b). This image is captured with 20 \times magnification, 1920 \times 1440 pixels, and 51 bands from 420 to 720 nm at 6 nm. Since the spatial resolution is too large to optimize the MSFA pattern, we used an image measuring 512 \times 512 pixels shown in Fig. 6 (c), which is cropped from the center of Fig. 6 (b). The 51-band MSI is regarded as the original MSI, and we show the validation of the optimized MSFA by mosaicking and demosaicking the 51-band MSI.

First, the peak signal-to-noise ratio (PSNR) of the optimized MSFA is compared with some conventional empirical-designed MSFAs, which are described in [15]. Table I shows the PSNR of the demosaicked MSI. Here, to simply validate

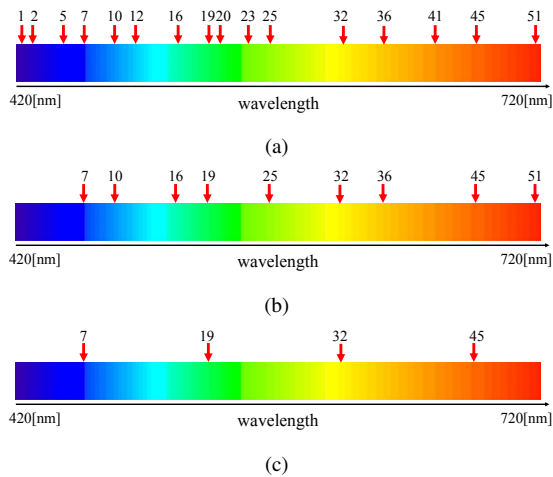


Fig. 7: Selected wavelengths after optimization: (a) 16 bands, (b) 9 bands, and (c) 4 bands.

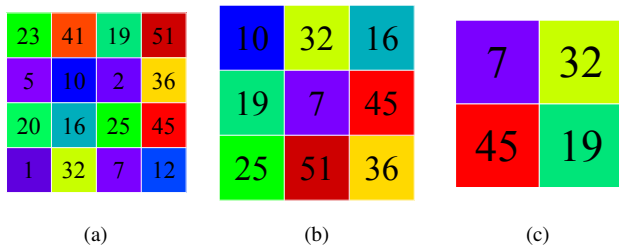


Fig. 8: Optimized MSFA pattern: (a) 16 bands, (b) 9 bands, and (c) 4 bands.

the proposed MSFA design, we use the conventional simple demosaicking method [6] for all MSFAs. From the result, we conclude that the proposed MSFA shows the highest PSNR. This implies that the proposed method can design better MSFA than the conventional methods. In particular, since the result of 9 bands is the highest value, we think that the best MSFA for recovering the 51-band MSI is not always a 51-band MSFA. If the number of measurement bands of MSFA is decreased, the intra-band measuring density becomes sparse. The balanced trade-off of the interpolation accuracy between the spatial and the spectral domain appears at 3×3 MSFA in Table I, and less than 10-band MSFA has the potential to become the best MSFA for pathological imaging.

In Table I, Shinoda et al. [15] is used as a benchmark that optimizes only the filter pattern. Since this method does not optimize the wavelengths, the PSNR between the proposed method and [15] corresponds to the performance of the wavelength optimization. The proposed wavelength optimization improves the PSNR by 0.482 dB in 3×3 MSFA.

Although Bayer and Raster chose the filter wavelengths at regular intervals, the proposed method chooses them by considering the MSE of the demosaicked image. The chosen wavelengths are shown in Fig. 7. Here, the numbers are the band indices, which is named from the short to the long

TABLE II: PSNR comparison (dB) between Brauers and MLDI demosaicking.

MSFA size	2×2	3×3	4×4
Proposed MSFA + MLDI	28.396	N/A	32.331
Proposed MSFA + Brauers	28.287	31.432	31.259

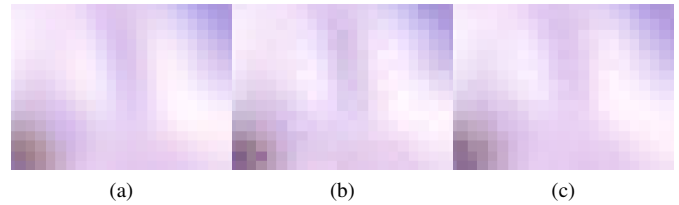


Fig. 9: Comparison of demosaicked RGB images: (a) Original, (b) 3×3 MSFA design and Brauers' demosaicking [6], and (c) 4×4 MSFA design and MLDI demosaicking.

wavelengths in the 51-band MSI. From Fig. 7, the chosen n bands are not always at regular intervals. This is because the proposed algorithm chooses bands where the error of the Wiener estimation is comparatively large. The optimized pattern is shown in Fig. 8. The closer bands in the wavelength domain are comparatively distant from each other in the spatial domain, and similar results were confirmed in [15]. The proposed pattern is not a regular pattern such as the Bayer pattern, but it could be one of the best solutions because the wavelength intervals are not constant.

Table II shows the PSNR comparison between Brauers and MLDI demosaicking. The proposed MLDI outperforms Brauers, and the PSNR is higher than that of Brauers in 4×4 . Here, 3×3 is N/A because the proposed MLDI can only apply to $2x \times 2x$ MSFA. Since 3×3 MSFA has the best performance, according to Table I, the application of MLDI to 3×3 MSFA is an important future challenge.

The original and demosaicked images are compared in Fig. 9. Here, these images are converted to an sRGB image from the demosaicked MSI. Fig. 9(a) shows the original image, (b) the demosaicked image obtained using the optimized 3×3 MSFA and Brauers' demosaicking, and (c) the demosaicked image obtained using the optimized 4×4 MSFA and MLDI. Although stepped noise can be seen in Fig. 9(b), the noise is improved in Fig. 9(c). However, we can see a little noise in Fig. 9(c). To compare more details in the spectral domain, we show the spectra of the cytoplasm and the nuclear region in Fig. 10. Here, "samples" refer to the measured bands in MSFA. The recovered spectra of the proposed method form a similar curve as the original, but the details differ from the original in both Fig. 10(a) and (b). In particular, around 550-600 nm, the spectra cannot recover the original curve because the sampling point does not exist within this range. The bands within 550-600 nm were not sampled by MSFA because the estimation error is comparatively small, but the loss of the bumps may lead to serious problems if the original spectrum within 550-600 nm has significant information for a

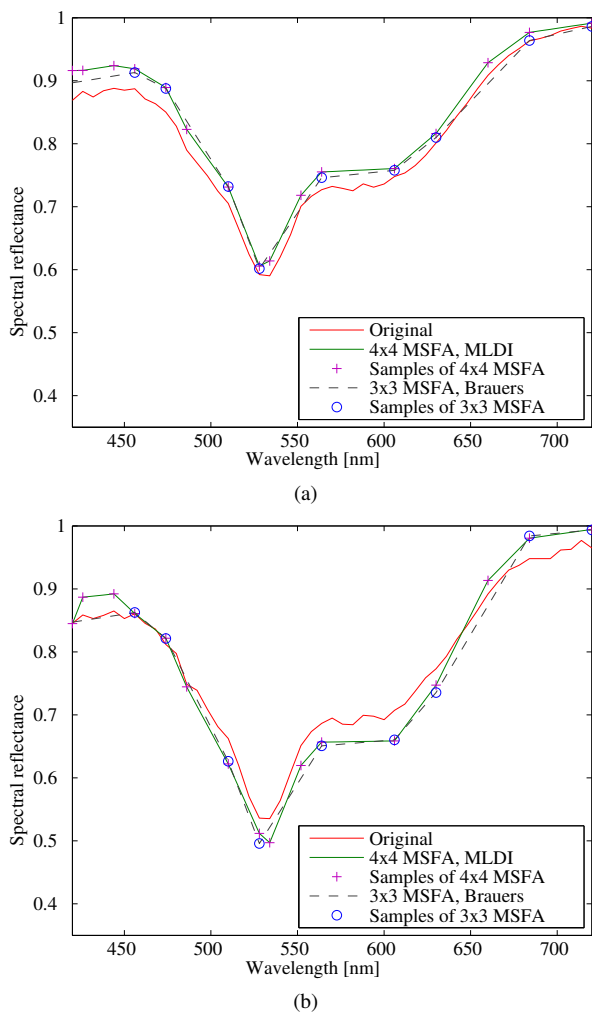


Fig. 10: Comparison of the spectrum: (a) cytoplasm region and (b) nuclear region.

TABLE III: PSNR (dB) of Fig. 11 (a) by using different MSFAs.

MSFA of Fig. 11 (b)	MSFA of Fig. 8 (b)	Bayer	Raster
31.411	31.168	31.033	30.941

pathological diagnosis. In the future, the meaningful bands for a pathological diagnosis should be clarified, and the proposed method should be modified to preferentially choose such meaningful bands.

For evaluating the effectiveness of the optimized MSFA in Fig. 8 (b), we use another test image. Fig. 11 (a) shows a different pathological image captured from C054 slide. Fig. 11 (b) and (c) show the optimized MSFA and wavelengths. In comparison between Fig. 8 (b) and Fig. 11 (b), three wavelengths are different but other six wavelengths are almost identical. Since many of the optimized wavelengths are almost identical between these images, a trained MSFA by using a certain pathological image can be potentially applied to other pathological images. Table III shows the PSNRs of Fig. 11 (a)

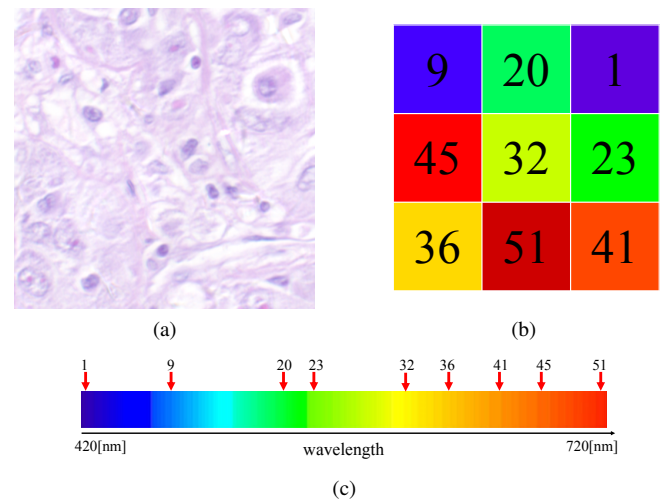


Fig. 11: Different test image captured from C054 slide. (a) 512×512 pixels, RGB image. (b) Optimized 3×3 MSFA. (c) Selected wavelength.

mosaicked with different four patterns. Here, we assume that Fig. 8 (b) is a trained MSFA. The optimized MSFA of Fig. 11 (b) shows the best performance, but the trained MSFA by Fig. 8 (b) shows also higher PSNR than the Bayer and Raster patterns. The PSNR difference between Fig. 8 (b) and Bayer is small, but the performance will be improved by increasing the number of training data set.

On the basis of these results, we conclude that the proposed MSFA design method, the obtained MSFA pattern, and the demosaicking are more effective for capturing multispectral pathological images than conventional methods. However, in the future, MLDI needs to be improved and the meaningful bands for a pathological diagnosis need to be clarified. Further, the problem is that the number of test samples is small. For the practical use of this method, the number of training images for designing MSFA should be increased so that the proposed method is applicable to various types of pathological images. Since H&E-stained pathological tissue has very few colors, MSFA for pathological images may contain a small number of bands even if the amount of training data is increased. In the future, we also intend to collect more training data and calibrate our MSFA pattern.

V. CONCLUSIONS

In this paper, we proposed a new MSFA design suitable for pathological images and evaluated its performance by using a demosaicking method. We used a 51-band MSI as the original image and simulated the mosaicking and demosaicking on a computer. The proposed MSFA pattern and demosaicking outperform conventional studies in terms of PSNR and can be applied to multispectral imaging for pathological diagnoses. In the future, we plan to improve the MLDI, clarify the meaningful spectral bands, and use more training data.

ACKNOWLEDGMENT

This work was supported by JSPS KAKENHI Grant Number 15K20899, the Center for Optical Research and Education of Utsunomiya University, and the Takahashi Industrial and Economic Research Foundation.

REFERENCES

- [1] T. Abe, Y. Murakami, M. Yamaguchi, N. Ohyama, and Y. Yagi, "Color correction of pathological images based on dye amount quantification," *Optical Review*, vol. 12, no. 4, pp. 293–300, July 2005.
- [2] M. Yamaguchi, H. Haneishi, and N. Ohyama, "Beyond red-green-blue(RGB): spectrum-based color imaging technology," *Journal of Imaging Science and Technology*, vol. 52, no. 1, pp. 10201-1–10201-15, Jan. 2008.
- [3] M. Tashiro, R. Yoshida, T. Miyazawa, Y. Murakami, M. Yamaguchi, N. Ohyama, and Y. Yagi, "H&E Digital Staining From the Multispectral Image of a Specimen Stained With Hematoxylin Only," *APIII 2009 Advancing Practice, Instruction, & Innovation through Informatics*, Abstract ID - 744, 2009.
- [4] P. A. Bautista, T. Abe, M. Yamaguchi, Y. Yagi, and N. Ohyama, "Digital Staining of Unstained Pathological Tissue Samples through Spectral Transmittance Classification," *Optical Review*, vol. 12, no. 1, pp. 7–14, Jan. 2005.
- [5] P. A. Bautista, and Y. Yagi, "Staining Correction in Digital Pathology by Utilizing a Dye Amount Table," *Journal of Digital Imaging*, vol. 28, no. 3, pp. 283–294, June 2015.
- [6] J. Brauers and T. Aach, "A color filter array based multispectral camera," *Proc. of Workshop Farbbildverarbeitung*, Oct. 2006.
- [7] Y. Monno, M. Tanaka, and M. Okutomi, "Multispectral demosaicing using adaptive kernel upsampling," *Proc. of IEEE International Conference on Image Processing*, pp. 3157–3160, Sept. 2011.
- [8] P. J. Lapray, X. Wang, J. B. Thomas, and P. Gouton, "Multispectral Filter Arrays: Recent Advances and Practical Implementation," *Sensors*, vol. 14, no. 11, pp. 21626–21659, Nov. 2014.
- [9] Y. Yanagi, K. Shinoda, M. Hasegawa, S. Kato, M. Ishikawa, H. Komagata, N. Kobayashi, "Multispectral Filter Array Considering Transparent Wavelength and Arrangement," *Forum on Information Technology*, Sept. 2015 (Japanese).
- [10] S. Ogawa, K. Shinoda, M. Hasegawa, S. Kato, M. Ishikawa, H. Komagata, N. Kobayashi, "Demosaicking Method for Multispectral Image Based on Spatial Gradient and Inter-Channel Correlation," *Forum on Information Technology*, Sept. 2015 (Japanese).
- [11] S. Kirkpatrick, C. D. Gelatt and M. P. Vecchi, "Optimization by Simulated Annealing," *Science*, Vol. 220, No. 4598, pp. 671–680, May 1983.
- [12] H. Haneishi, T. Hasegawa, A. Hosoi, Y. Yokoyama, N. Tsumura, and Y. Miyake, "System design for accurately estimating the spectral reflectance of art paintings," *Applied Optics*, vol. 39, no. 35, pp. 6621–6632, 2000.
- [13] W. K. Pratt and C. E. Mancill, "Spectral estimation techniques for the spectral calibration of a color image scanner," *Appl. Opt.*, vol. 15, no. 1, pp. 73–75, 1976.
- [14] Y. Murakami, M. Yamaguchi and N. Ohyama, "Piecewise Wiener estimation for reconstruction of spectral reflectance image by multipoint spectral measurements," *Appl. Opt.*, vol. 48, pp. 2188–2202, 2009.
- [15] K. Shinoda, T. Hamasaki, M. Hasegawa, S. Kato, and A. Ortega, "Quality metric for filter arrangement in a multispectral filter array," *Picture Coding Symposium*, pp. 149–152, Dec. 2013.